China Instrument and Control Society
Instrumentation
OPEN ACCESS
INSTRUMENTATION, Vol. 11, No. 1, March 2024 https://doi.org/10.15878/j.instr.202300161

Article

Integrated Test System for Large-aperture Telescopes Based on Astrophotonics Interconnections

Qichang An[1,*], Kun Wang[1,3], Xinyue Liu[1,3], Hongwen Li[1,3], and Jiakang Zhu[1,2,3]

[1] Changchun Institute of Optical Precision Machinery and Physics, Chinese Academy of Sciences, Changchun, Jilin 130033, China

[2] University of Chinese Academy of Sciences, Beijing 100039, China

[3] Jilin Key Laboratory of Intelligent Wavefront Sensing and Control, Changchun, Jilin 130033, China

[*] Corresponding author email: anjj@mail.ustc.edu.cn

Abstract: This study aims to improve the integrated testing of large-aperture telescopes to clarify the fundamental principles of an integrated testing system based on astrophotonics. Our demonstration and analyses focused on element-position sensing and modulation based on spatial near-geometric beams, high-throughput step-difference measurements based on channel spectroscopy, distributed broadband-transmittance testing, and standard spectral tests based on near-field energy regulation. Comprehensive analyses and experiments were conducted to confirm the feasibility of the proposed system in the integrated testing process of large-aperture telescopes. The results demonstrated that the angular resolution of the light rays exceeded 5 arcsec, which satisfies the requirements for component-position detection in future large-aperture telescopes. The measurement resolution of the wavefront tilt was better than 0.45 μrad. Based on the channel spectral method—which combined a high signal-to-noise ratio and high sensitivity, along with continuous-spectral digital segmentation and narrowband-spectral physical segmentation—a resolution of 0.050 μm and a range of 50 μm were obtained. After calibration, the measurement resolution of the pupil deviation improved to exceed 4% accuracy, and the transmission measurements achieved a consistency of over 2% accuracy. Regarding fringe-broadband interferometry measurements, the system maintained high stability, ensuring its operation within the coherence length, and robustly detected the energy without unwrapping the phase. The use of a projector for calibrating broadband-spectrum measurements led to a reduction in contrast from 0.8142 to 0.6038, which further validates the system's applicability in the integrated testing process of large-aperture telescopes. This study greatly enhanced the observational capabilities of large-aperture telescopes while reducing the integrated system's volume, weight, and power consumption.

Keywords: curvature sensing; wavefront aberration; astrophotonics; large-aperture telescope

Citation: An, Qichang, Kun Wang, Xinyue Liu, Hongwen Li, and Jiakang Zhu. 2024. "Integrated Test System for Large-Aperture Telescopes Based on Astrophotonics Interconnections." *Instrumentation* 11, no. 1. https://doi.org/10.15878/j.instr.202300161.

0 Introduction

Astronomical observation is evolving toward multi-messenger and multi-platform approaches. To achieve higher spatial resolution and detection capabilities, the telescopes tend to have enhanced spatial resolution, stronger light-collecting abilities, and larger fields of view (FoV). Future ground-based telescopes are likely to be in the 30-m to 40-m class; however, the telescope apertures used in the development of the James Webb Space Telescope (JWST) have transitioned from the 2-m to 6-m class[1-4].

Future habitable-planet imaging observatory projects, as well as general-purpose space telescopes, are

expected to contribute to exoplanet exploration. In 2009, the United States launched the Kepler space telescope, initiating its space-based exoplanet exploration program. In 2018, the Transiting Exoplanet Survey Satellite (TESS) space telescope was launched. Launched in 2013, the Gaia space telescope explored exoplanets through astrometric measurements. The JWST has a larger aperture and more powerful end detectors than the Hubble Space Telescope (HST), enabling the exploration of the first light formations of the universe and the investigation of dark matter and dark energy through gravitational lensing[5, 6]. Additionally, the 3.5-m Herschel Space Observatory offers enhanced insight into the early characteristics of the universe through its infrared-band detection. The US Space Interferometry Mission PlanetQuest (SIM-PQ)—a space-borne instrument that can perform astrometry to μarcsec precision on the visible light from a large sample of stars in our galaxy—aims to employ visible-light wavelengths to take large field-of-view measurements with a 6-m baseline. Consequently, its angular measurement resolution is better than 4 μarcsec under 15°-field-of-view.

The construction of these large-aperture telescopes not only expands human understanding of the cosmos's initial dark periods—allowing the observation of the "first light"—but also facilitates the effective exploration of habitable exoplanetary systems through refined spectroscopic analysis. High-precision spectral-resolution tests can identify the spectral changes caused by the apparent velocity variations of exoplanets during transits across their host stars (manifested as alternating blueshifts and redshifts).

The direct imaging of exoplanets necessitates the use of long-baseline planet interferometry technology, with the fine characterization of exoplanets being based on the visible-light and infrared wavelength bands. Integrated testing is a critical phase in ensuring that the telescope performance meets the design specifications. Throughout the assembly, adjustment, disassembly, transportation, and recovery processes, system testing is essential. For example, the Herschel Space Telescope used discrete phase sub-apertures for integrated system testing, achieving a final test precision of 400 nm (λ = 80 μm)[7].

At present, LAMOST, the world's largest spectral survey, has entered the medium-resolution survey phase (R = 7500), acquiring massive volumes of data on stellar physical parameters and chemicals, and compiling multidimensional information in conjunction with existing digital survey projects[8]. Prior to each operation, a Hartmann wavefront sensor is used to calibrate and debug its spherical mirror to ensure system optical quality[9].

The Center for High Angular Resolution Astronomy (CHARA)—one of the earliest planet interferometers—comprises six telescopes, each with a 1-m aperture. Its longest baseline can reach 300 m, covering the visible and near-infrared bands. The Keck Telescope—which comprises two 10-m segmented telescopes—uses single-mode fibers for interconnection, forming a 140-m baseline planet interferometer. Subsequently, the conceptual Optical Hawaiian Array for Nanoradian Astronomy (OHANA) interferometer array, which connects multiple telescopes, was proposed. The Very Large Telescope Interferometer (VLTI) at the European Southern Observatory comprises four 8.2-m telescopes and four 1.8-m telescopes, offering baselines of up to 100 m. After wavefront correction using adaptive optics, it can synthesize beams in the visible, near-infrared, and mid- and long-wavelength bands. Long-baseline interferometry enables precise angular measurements of celestial bodies, offering considerable value in exoplanet detection and interstellar-environment examination.

Additionally, with the expanding field-of-view of telescopes, multi-field cooperative detection has evolved as the development direction for the integrated testing of future large-aperture telescopes. The combination of large apertures and adaptive optics allows telescopes to observe more refined cosmic structures, contributing to observations related to black holes, dark matter and energy, and Earth-like planets.

However, high-resolution adaptive-optical systems require higher standards for pupil alignment. The gradual vignetting of the pupil can alter the weight of the wavefront sensing and correction stages, leading to non-converging corrections. Moreover, a misaligned system pupil can introduce off-axis stray light, compromising the ultimate depth of the high-contrast imaging process. In the context of large-aperture wide-field systems, the misalignment of telescope optical components can exacerbate off-axis aberrations. This, combined with the intrinsic lack of stiffness in large-aperture systems, can render observations impossible.

Consequently, active control of optical components and terminals is greatly needed. Digital sky-survey telescopes (such as the Sloan Digital Sky Survey (SDSS) and Large Synoptic Survey Telescope (LSST)) use multiple sets of filters to facilitate multi-wavelength and multimode observations across diverse spectral segments of the universe. Through analysis of the spectral and photometric characteristics, important parameters (such as cosmological constants) can be determined[10-12].

High-precision astronomical detectors currently grapple with several major challenges. First, the back-end fringe resolution is constrained because of limitations in the system's pixel resolution. Moreover, increased focal lengths result in a larger system volume, weight, and vulnerability to external perturbations. Accomplishing high phase-positioning accuracy remains elusive with lower pixel resolutions. Furthermore, high-contrast imaging necessitates the application of nulling interference and the reorganization of wavefront phases. When using bulk optical components for beam bending and redirection, physical and volumetric constraints limit the number of measurable paths.

In this study, to address the drawbacks of traditional free-space optical propagation—which is highly susceptible to atmospheric disturbances and environmental vibrations, making direct wavefront error-testing impossible—a fiber-coupled system was introduced. This system mitigated mechanical and spatial constraints and simultaneously decreased the surface quality and rigidity requirements of the back-end mechanisms. Ultimately, this allowed for the optical alignment and testing of large-aperture telescopes at a reduced cost, thereby reducing reliance on large-aperture collimators.

Astrophotonics is an emerging field that has flourished in recent years. By leveraging technologies such as optical communication, it has greatly enhanced the measurement throughput and cost-effectiveness of integrated tests, while reducing the system's volume and weight, thereby enhancing its suitability for space-based interferometry systems.

Wavefront detection is the most direct and effective evaluation method for large-aperture systems. Traditional zero-position detection necessitates the independent design of compensating optical paths. The component alignment and accuracy tracing are challenging; in addition, it is difficult to process and inspect large-aperture standard plane mirrors.

The GRAVITY interferometric synthesizer of VLTI utilizes astrophotonics technology, achieving a spatial resolution of 10 μarcsec in the near-infrared band[13]. The University of Sydney in Australia has achieved high-contrast interferometry at the level of 10^{-3} through the development of an astrophotonics nulling modulator (Guided-Light Interferometric Nulling Technology (GLINT) project)[14].

In terms of spectral detection, using fiber-interconnection systems can rearrange the aperture of the planar light source for further spectrum calibration and analysis. The use of wavelength-division multiplexing devices allows the system's wavebands to be separated.

The next generation of planetary interferometers will take the form of astrophotonics, where spectroscopy, aperture rearrangement, and interferometric synthesis will be performed using photonic devices; this will facilitate high-resolution and high-contrast imaging. The front-end beam-collection part of the system implementation architecture can still employ large-aperture telescopes for collecting beams, which, after alignment and adjustment, can be coupled into waveguides.

1 Theory: Basic Principles

Fiber-optic interconnection systems can realize spectral splitting at any ratio, as well as highly integrated optical folding. They can also generate light beams in any direction within a small range, and effectively enhance the detection efficiency and throughput. Moreover, waveguide optical splitters can facilitate the arbitrary proportion of splitting and combining signals of identical wavelengths.

Consequently, based on the Hartmann method, a geometrical optical wavefront-calculation method (known for its non-interference, high robustness, and strong aperture adaptability) can be used in conjunction with aperture coding technology. Thus, information-sensing throughput can be enhanced to help isolate and suppress multi-parameter and multi-level errors, enabling the acquisition of high-precision sub-aperture data.

In the realm of optical interconnections, optical pathways replace data circuits between chips, coupling, splitting, and distributing the optical communication signals. Optical wavelength-division multiplexing (WDM) techniques can transmit multiple optical wavelengths simultaneously. Consequently, by employing geometric phase materials in conjunction with spectral confocal principles, wavefronts can be detected. Further, the spectrum can be calibrated using wavelength-division multiplexers. Thus, spectral response and transmittance curves can be obtained in two dimensions using light-intensity inputs at different frequencies and spatial distributions. Concurrently, they form a conformal structure in the system to enhance the system perception capability.

Moreover, with the advances in integrated optics technology, the cost and scale of area-array detectors are rapidly decreasing, enabling large-scale spectral testing. In contrast to using linear-array detectors, the influence of the link process on the intensity response-function calibration of area-array detectors can affect the system's light-intensity detection, as well as its calibration accuracy. For transmittance detection, edge rays can be employed for optical-pupil alignment testing. Pupil plane information is acquired through scanning collection, which can be analyzed to obtain transmittance information.

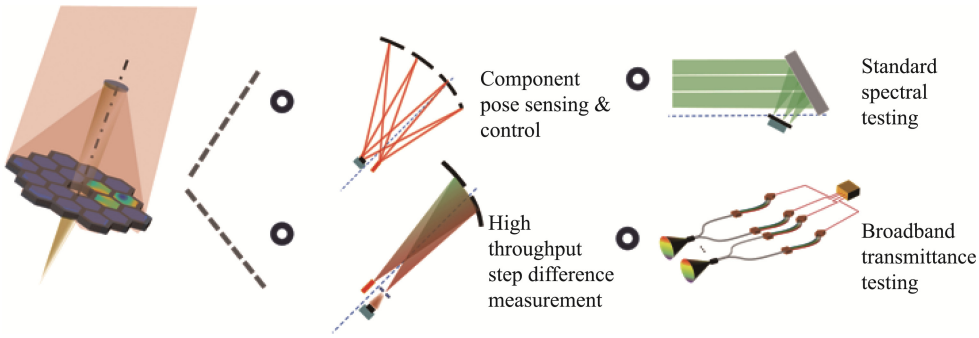

Fig.1 Schematic of integrated detection of large-aperture telescopes based on fiber-optic interconnections

The following functions can be achieved with a fiber-optic interconnection system:

• Element-position sensing and modulation, based on spatial near-geometric beams;

• High-throughput step-difference measurements based on channel spectroscopy;

• Distributed broadband-transmittance testing;

• A standard spectral test system based on near-field energy regulation.

2 Methods: Verification of Fiber-Interconnection Feasibility

2.1 Component-position Testing

Using the deflection effect of geometric beams and coordinating with optical models for joint simulation, the positional information of characteristic rays on the target surface can be used to detect a system misalignment. The light source can be positioned at the system's entrance pupil or above the vane, enabling monitoring of optical component position changes within the system.

Rays emitted at different positions and angles can be imaged on the same system surface, as shown in Fig.2. Quasi-geometric rays are scanned and input at the entrance pupil of a telephoto collimator, capturing its precise image. A comparison reveals that the position of the incident target surface remains constant when the rays are parallel. However, when the rays are inclined, the target surface position changes.

By directing rays at different positions in the optical pupil and combining the related measurements of the image-point positions, the angular resolution of the rays is observed to be more than 5 arcsec, meeting the detection requirements of component positions in future large-aperture telescopes. Here, the resolution information is obtained jointly by the pixel resolution (20 μm) and focal length (1 m).

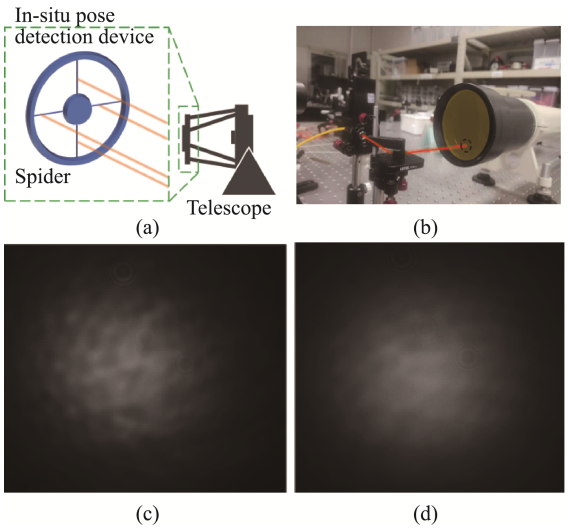

Fig.2 Fiber-optic interconnect position testing verification: (a) Testing principle, (b) Experimental platform, and (c)–(d) Different incidence positions and focal-plane light intensities

Taking the mixed aberration of spherical aberration and defocus as an example, where a_4 and a_{11} are Zernike coefficients, and x and y are Cartesian coordinates:

$$\Phi = a_4\rho^2 + a_{11}\rho^4 = a_4\left(x^2+y^2\right) + a_{11}\left(x^2+y^2\right)^2 \quad (1)$$

The slope in the x-direction of the wavefront can be expressed as follows:

$$\frac{\partial}{\partial x}\Phi = 2xa_4 + a_{11}4x\left(x^2+y^2\right) \quad (2)$$

The slope in the y-direction of the wavefront can be expressed as follows:

$$\frac{\partial}{\partial y}\Phi = 2ya_4 + a_{11}4y\left(x^2+y^2\right) \quad (3)$$

For a spherical segmented mirror, the incident light is set at its radius of curvature, and the detector is set at the corresponding curvature center. By measuring the change in the position of the reflected light spot to calculate the slope, the surface of the segmented spherical mirror can be obtained. Test scenes and resolution testing based on near-geometric beams are shown in Fig.3.

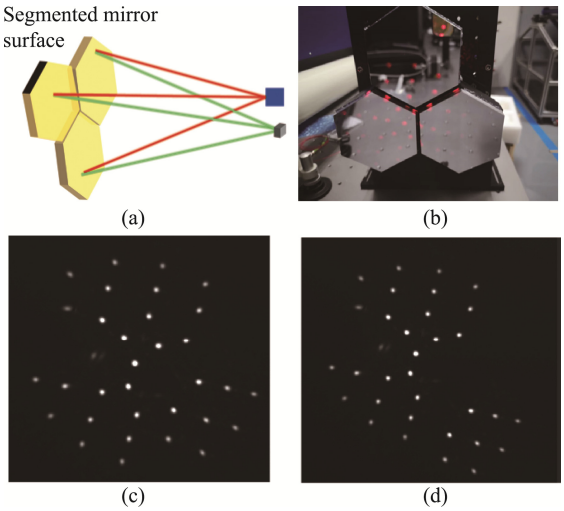

Fig.3 Test scenes and resolution testing based on near-geometric beams

The wavefront's slope can be determined by sparse sampling between two spatial points and coherent synthesis. Moreover, based on the interference fringes, the system wavefront can be estimated.

2.2 Piston-error Testing

The visibility associated with different sizes of sub-apertures does not uniformly align with the phase variations occurring at the system boundaries. This inconsistency can be attributed to alterations in the modulation relationship between the circular aperture diffraction and interference, owing to changes in the aperture sizes. The physical interval (δ) can be expressed as follows:

$$\lim_{\lambda_1\to\lambda_2} 2\pi\frac{\delta}{\lambda_1} - 2\pi\frac{\delta}{\lambda_2} = \lim_{\lambda_1\to\lambda_2}\Delta\varphi \quad (4)$$

Based on the definition of partial derivatives, the relationship between the final actual interval and the partial derivative of the stripe intensity can be obtained, as follows:

$$\frac{\partial\left(2\pi\frac{\delta}{\lambda}\right)}{\partial\lambda}=-2\pi\frac{\delta}{\lambda^2}=\frac{\partial\mathbf{I}\left(x,\,y\left(\lambda\right)\right)}{\partial\lambda} \tag{5}$$

The fiber interconnection system facilitates the adjustment of the position and posture of large-aperture radio or optical telescope sub-mirrors. By employing the principles of broadband interference and adhering to coherence-length limitations, the system can ensure precise relative positioning among the sub-mirrors.

For segmented mirrors, multiple-wavelength beams are incident on the local aperture of their segmented seams, and a dispersion element is used to disperse the reflected light. Step-difference tests for multiple wavelengths below red/green visible light are shown in Fig.4.

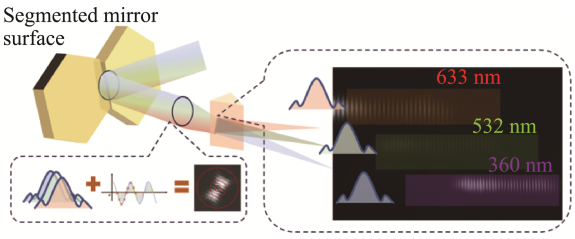

Fig.4 Step-difference test for multi-wavelengths below red/green visible light

Moreover, the system can conduct spatial angular spectroscopy and measure the relative heights, based on the received light rays. These measurements can be used to resolve the overall surface shape of the system. Based on the channel spectral method—which combines a high signal-to-noise ratio and high sensitivity, along with continuous-spectral digital segmentation and narrowband-spectral physical segmentation—a resolution of 0.050 μm and range of 50 μm can be obtained simultaneously.

In cases involving larger sub-apertures, the formed interference fringes are subject to modulation, owing to circular aperture diffraction, decreasing the light intensity at specific fringe positions. Under these circumstances, the position of maximum contrast does not align with the coarse collimation position of the system; this introduces ambiguity in the measurements. Consequently, a methodology for discerning the maximum pupil diameter emerges from this observation, based on the distinctive nature of contrast variation.

An evaluation of the light intensity within an individual circular sub-aperture (internal to the mirror) reveals that its external envelope closely resembles a Gaussian function. However, owing to the asymmetry of the boundary sub-aperture, a unilateral deviation is evident in the light spot, which approximates a half-sided Gaussian function when compared to the conventional Gaussian function. This particular characteristic necessitates the preservation of the system's collimated state during the fine collimation process.

In the pre-interference state, the fringe contrast is considerably diminished, thus preventing high-precision tilt measurements of the system. Concurrently, the phenomenon of partial interference fringes coupled with light-intensity crosstalk complicates the centroid-extraction process and induces a resultant offset, expressed as follows:

$$\begin{aligned}E=&\int_{-B/2-D/2}^{-B/2+D/2}e^{j(2\pi x\theta/\lambda+2\pi\delta/2\lambda)}\mathrm{d}x+\int_{B/2-D/2}^{B/2+D/2}e^{j(2\pi x\theta/\lambda-2\pi\delta/2\lambda)}\mathrm{d}x=\\&e^{j(\pi\delta/\lambda)}\int_{-B/2-D/2}^{-B/2+D/2}e^{j(2\pi x\theta/\lambda)}\mathrm{d}x+e^{j(-\pi\delta/\lambda)}\int_{B/2-D/2}^{0}e^{j(2\pi x\theta/\lambda)}\mathrm{d}x=\\&e^{j(\pi\delta/\lambda)}\frac{1}{j\left(2\pi\theta/\lambda\right)}e^{j(2\pi x\theta/\lambda)}\Big|_{-B/2-D/2}^{-B/2+D/2}+\\&e^{j(-\pi\delta/\lambda)}\frac{1}{j\left(2\pi\theta/\lambda\right)}e^{j(2\pi x\theta/\lambda)}\Big|_{-D/2}^{0}=\\&\frac{\sin\left(k\theta\frac{D}{2}+k\delta/2\right)}{k\theta D/2}\cos\left(k\theta\frac{D}{2}+k\delta/2\right)\end{aligned} \tag{6}$$

The final light-intensity distribution can be expressed as follows:

$$\mathbf{I}=\left|E\right|^2=\left[\frac{\sin\left(k\theta\frac{D}{2}+k\delta/2\right)}{k\theta D/2}\right]^2\cos^2\left(k\theta\frac{D}{2}+k\delta/2\right) \tag{7}$$

Here, correlation operations can be used for precise position extraction. In the subsequent fine-collimation process, the tilt of the fringes can be used for system adjustment. Once the system fringes enter the state of optimal visibility (reaching an extremum), the fringe phase can be used for coarse collimation adjustments (broadband method).

Moreover, the interference fringes formed using spatial optical paths are modulated by the aperture-function diffraction pattern (such as the two-dimensional *sinc* function produced by a square aperture), which results in a faster contrast reduction, thus limiting the number of fringes usable for wavefront computation. The fringes generated from optical waveguides appear more uniform and are less affected by aperture modulation. Thus, sufficient fringe periods can be formed to ensure the accuracy of broadband fitting.

Based on the above analysis, it can be concluded that when different apertures undergo local interference, coupling adjustments will be made between the aperture function and interference fringes. Different interference apertures will generate corresponding fringe patterns. The verification results of fringes with different baseline lengths are shown in Fig.5.

2.3 Transmittance Testing

Optical waveguides can be used to form photonic

lead-ins, facilitating the interconnection of receiving telescopes via optical fiber and establishing interference fringes through integrated photonic waveguide interference. A prototype of a planet interferometer, predicated on integrated photon interference, is depicted in Fig.6, targeting the simulation of remote objects. Consequently, interference fringes corresponding to various sampling positions can be obtained.

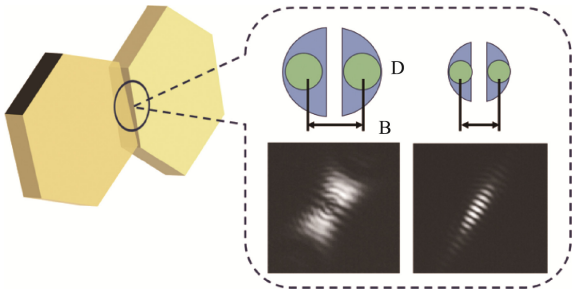

Fig.5 Verification results of fringes with different baseline lengths

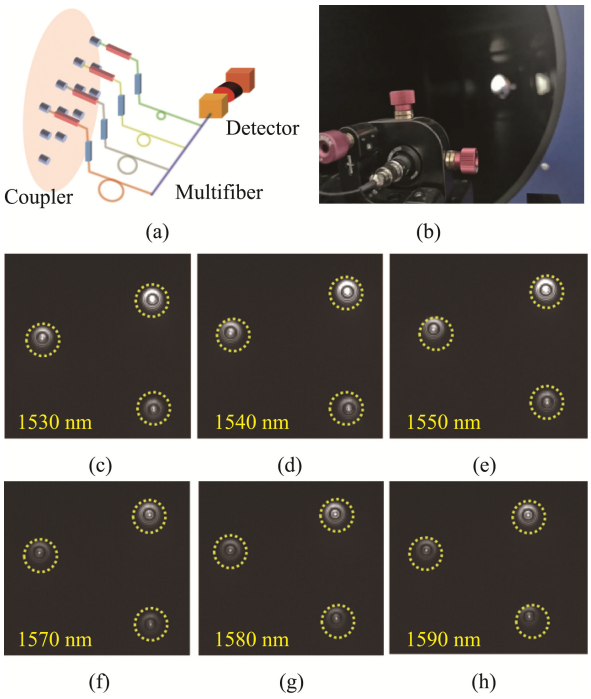

Fig.6 Verification of the fiber-optic interconnect transmittance testing: (a) Test principle, (b) Experimental platform, and (c)–(h) Focal-plane light intensity

By testing the contrast of the fringes, the angular radius of the target can be determined. Furthermore, these calculations enable the extrapolation of the system's intrinsic characteristics. By combining these findings with distance-measurement outcomes, the object's actual dimensions can be determined. In the most practical use-case scenario, the system can be solidified with multiple sub-apertures, and the angular radius of the target can be confirmed, based on the interference contrast between different sub-apertures.

Transmittance testing effectively enhances the uniformity of system measurement. Through the calibration of light intensity and spectra, the influence of various film systems and dust on the overall transmittance of the system can be determined.

The optical-fiber interconnection system can be leveraged, using strategies to effectively suppress stray light, mitigating its influence on spectral and phase measurements. Concurrently, employing the optical-interconnection system enables tomographic measurements of the optical pupil, focusing on changes in the light intensity at peripheral regions to test the alignment of the system's optical pupil.

Specifically, based on the initial light-intensity calibration, a slight position offset occurs when the light intensity deviates; however, its distribution changes with the tilt of the components. Consequently, by employing the optical-fiber interconnection system, tomographic measurements of the light intensity can be conducted at various pupil positions. This enables the acquisition of optical-pupil alignment data and multi-pupil posture information using the least-squares method. Compared to space-division multiplexing using a photonic lantern, mode overlap can be avoided.

After calibration, the deviation measurement resolution of the optical pupil exceeded 4%, and the consistency of the transmission-rate measurement accuracy was more than 2%.

2.4 Spectral Testing

The use of multiple dense rows of optical waveguides can regulate the incoming light field, and through jointly regulating the intensity of each mode, the outgoing light field can be uniformly projected. The uniformity of the optical-field projection can be further enhanced by considering the exit optical field of the system through mirror contrast.

Similar to the optical phased-array method, this study modulates the overall exit wavefront through mode control between each channel. For the optical phased array, the overall exit wavefront direction can be modulated primarily through the modulation of the system phase. Regarding mode control, the exit-light intensity and mode-field distribution can be modulated by modulating the propagation efficiency of each order mode in the waveguide.

The incoherent measurement mode is comparable to a large-aperture, small-field-of-view fiber-optic spectral system. The mode capitalizes on prolonged integration times on specific targets to extract detailed spectral information. Synthetic detection experiments can be conducted for incoherent detection.

Initially, the system's pointing direction is adjusted, after which, multimode fibers are used for capturing and channeling light beams into the detection apparatus, such as spectrometers and point detectors. The spectral characteristics of the target can be obtained through the energy decomposition in the spectral domain. Collimators are used to simulate distant targets, and single-mode

fibers at precise points in the collimators can be used to represent distant targets. An adjustable laser can be employed to modulate the light intensity and frequency, with detection occurring at the back end.

Additionally, discrepancies in the propagation modes of light rays of diverse wavelengths within the waveguide can lead to variations in the attenuation of differing light intensities. Consequently, to ensure the accuracy of spectral-intensity measurements, mode scrambling is necessary at the back end of the multimode fibers. Employing a mode scrambler during the calibration process greatly enhances the consistency of broadband spectral-intensity measurements, with improvements exceeding 30%.

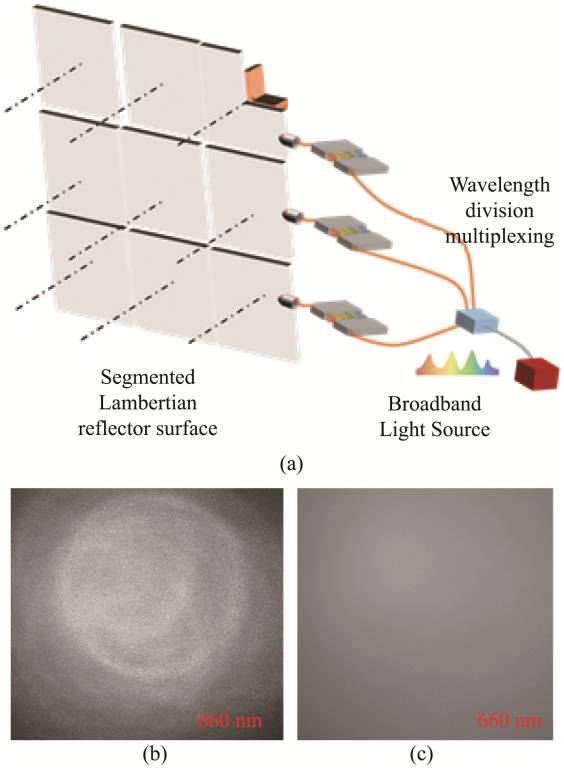

Fig.7 Near-field light-source control cross-comparison verification experiment: (a) Near-field controlled light-intensity projection device, (b) Light-intensity distribution before control, and (c) Light-intensity distribution after control

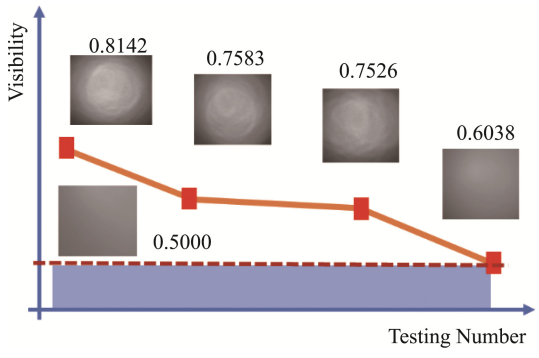

Fig.8 Decline of light-intensity contrast during the control process, as well as a comparison with the integrating sphere

In the experimentation phase, an integrating sphere was used to flat-field calibrate the system. After this, a projection system was employed to conduct spectral measurements. The strategy of employing densely packed multimode fiber-optic waveguides, phased arrays, and aperture synthesis culminated in the successful spectral detection and calibration of the system. A noticeable reduction in contrast, from 0.8142 to 0.6038, was observed.

In the spectral-measurement architecture based on optical waveguides, the interaction between the light-propagation modes and spectral-measurement link significantly influences the precision and sensitivity of the final spectral measurements. In this study, a characteristic analysis of the light of different modes in the optical-interference method was conducted across various spectral sections.

The spectral-projection system demonstrated a notable enhancement in light dispersion and uniformity. The use of a mode scrambler, as shown in Fig.7(b)–7(c), assisted in the suppression of multimode interference emitted by the multimode fibers. Consequently, the method of combining multimode fiber emission with a mode scrambler could mitigate the systemic mode interference and spectral drift caused by optical interference, substantially enhancing the efficiency and accuracy of the spectral-measurement system.

3 Results and Discussion

Coherent-light diffraction and stray light under the fiber-optic interconnection architecture are key factors constraining the sampling density and reconstruction accuracy in detection. Consequently, based on the principle of aperture coding, balancing the sampling efficiency, reconstruction accuracy, and coherent crosstalk among various paths is fundamental to achieving high-precision perception of large-aperture transmitted wavefronts.

In this study, desktop experiments were used to verify the principle and scheme testing. For each key technology, a minimal system used to verify the principle was individually set up, and data were collected. A statistical expression of the system characteristics was obtained through analysis, validating the feasibility of the scheme.

The application of a strategy characterized as “assessing larger systems through smaller ones,” can facilitate swift, *in-situ* validation of critical performance metrics, thereby mitigating the repercussions of external hardware interference. This method involves conducting a meticulous pupil-slicing examination of the parallel light projected by the system. Building upon the acquired data on wavefront slopes provides an opportunity to reconstruct and estimate the wavefront aberrations, thereby ensuring an evaluative foundation to confirm the system’s operational excellence.

Moreover, the method can also be applied to

transmission-system inspections. Transmission wavefront detection is the most direct and effective method for evaluating the performance of lens groups. Traditional zero-position detection requires the separate design of a compensatory optical path, which not only makes component alignment and precision tracing difficult but also complicates the manufacturing and inspection of large-aperture standard mirrors.

Using the architecture of fiber- interconnection, combined with the advantages of slope-stitching measurements (such as inherent baselining and disturbance resistance), this method aims to achieve high-precision, *in-situ* determination of various parameters in large-aperture systems.

4 Conclusions

To improve resolution and sensitivity, future spatial optical systems will have increasingly larger apertures. Existing large-aperture spatial optical systems have already reached the meter-size class, and projections indicate the launch of 2-m or even 6-m aperture systems in the future. Consequently, the traditional full-aperture optical testing methods used for these colossal spatial optical systems have encountered bottlenecks in spatial span and cost efficiency.

By using a pentaprism to emit light beams (which eventually form light spots on the focal plane) and transforming the incident light spectrum, this study established a mapping relationship between the incident and emerging light spectra, thus obtaining a single-aperture response. After obtaining the sub-aperture response, the next sub-aperture position was measured. After acquiring the data, we could approximate the full aperture's equivalence by smoothing the overlapping boundaries.

The sub-aperture stitching method allowed for the digital synthesis of small-aperture detection, which considerably lowered the cost of executing large-aperture optical system detection. Consequently, the proposed method could be positioned as a mainstream technology for the quality inspection of future large-aperture spatial optical systems.

The proposed method adopted astrophotonics techniques, aligning closely with actual on-site testing conditions to facilitate *in-situ* calibration testing of large-aperture optical systems. Employing *in-situ* testing enabled the confirmation of system performance under actual operational and calibration conditions, serving as an essential enabling technology to ensure long-term and stable system-performance maintenance.

Additionally, by leveraging bulk optical components and photon-integrated interference comparisons, photon interference facilitated the procuring of broader and more linear fringes. Using photonic devices for system integration fostered the acquisition of high-quality fringes, circumventing the additional optical path lengths introduced by the deflection of multi-faceted reflectors. The reduced system weight and volume enhanced its embedding within the system's optical pathways.

Ultimately, for the integrated testing of large-aperture telescopes, the angular resolution of the light rays can be greater than 5 arcsec, which meets the detection requirements for the positioning of components in future large-aperture telescopes. Moreover, the measurement resolution for wavefront tilt can be greater than 0.45 μrad.

After calibration, the measurement resolution for pupil deviation exceeds 4%, and the consistency of the transmission-rate measurement accuracy is greater than 2%. A mode scrambler was used to calibrate the broadband-spectrum measurement, and the contrast decreased from 0.8142 to 0.6038.

The proposed method exhibits superior adaptability to the pressing demands of future high-efficiency, mass-scale integrated system testing, thus overcoming the prevailing challenges associated with balancing cost-efficiency and performance optimization.

Author Contributions:

Conceptualization, Qichang An; Data curation, Qichang An and Kun Wang; Formal analysis, Qichang An; Funding acquisition, Qichang An; Investigation, Jiakang Zhu; Methodology, Qichang An and Kun Wang; Project administration, Qichang An, Xinyue Liu and Hongwen Li; Resources, Qichang An; Software, Qichang An; Supervision, Xinyue Liu and Hongwen Li; Validation, Qichang An and Kun Wang; Visualization, Qichang An and Jiakang Zhu; Roles/Writing original draft, Qichang An; Writing review & editing, Qichang An and Jiakang Zhu.

Acknowledgments

Thanks Dr, Hu and Dr.Wang for the help in testing.

Funding Information

This work was supported by the National Natural Science Foundation of China (Grant No. 12133009), the Youth Innovation Promotion Association of the Chinese Academy of Sciences (Grant No. 2020221), and the Science and Technology Development Plan of Jilin Province (Grant No. 20220402032GH).

Data Availability:

The authors declare that the main data supporting the findings of this study are available within the paper and its Supplementary Information files.

Conflict of Interest:

The authors declare no competing interests.

Dates:

Received 02 November 2023; Accepted 09 January 2024; Published online: 31 March 2024.

References

[1] Spergel, D., Gehrels, N., Breckinridge, J., *et al.* Wide-Field Infrared Survey Telescope- Astrophysics Focused Telescope Assets WFIRST- AFTA Final Report. *Physics* (2013).

[2] Bolcar, M., *et al*. The Large UV Optical Infrared Surveyor (LUVOIR): Decadal Mission concept design update. *SPIE Optical Engineering + Applications* Vol. 10398 (2017).

[3] Fortney, J., Kataria, T., Stevenson, K., *et al*. The Origins Space Telescope: Towards an Understanding of Temperate Planetary Atmospheres. (2018).

[4] Kim, D. W., Esparza, M., Quach, H., *et al.* Optical technology for future telescopes. In *Proceedings of the Fourth International Conference on Photonics and Optical Engineering*. International Society for Optics and Photonics, 11761: 1176103 (2021).

[5] Postman, M., *et al.* Using the ISS as a testbed to prepare for the next generation of space-based telescopes. *SPIE Astronomical Telescopes + Instrumentation* Vol. 8442 (2012).

[6] Sabelhaus, P. A., Decker, J. E. An overview of the James Webb space telescope (JWST) project. In *Proceedings of SPIE Optical, Infrared, and Millimeter Space Telescopes*. International Society for Optics and Photonics, 5487: 550-563 (2004).

[7] Benielli, D., Polehampton, E., Hopwood, R. *et al.* Herschel SPIRE FTS spectral mapping calibration. *Exp Astron* 37: 357-367 (2014).

[8] Su, D. Q., Cui, X., Wang, Y. N., Yao, Z. Q. Large-Sky-Area Multiobject Fiber Spectroscopic Telescope (LAMOST) and its Key Technology, Proc. SPIE 3352, *Advanced Technology Optical/IR Telescopes VI* (1998).

[9] Briguglio, R., Quirós-Pacheco, F., Males, J. R. *et al*. Optical calibration and performance of the adaptive secondary mirror at the Magellan telescope. *Sci Rep* 8, 10835 (2018).

[10] Biasi, R. *et al.* E-ELT M4 adaptive unit final design and construction: A progress report. In *Adaptive Optics Systems V*, Vol. 9909 of *Proc. of SPIE*, 99097Y (2016).

[11] Wei, H., Hu, H., Yan, F. *et al.* Multi-beam array stitching method based on scanning Hartmann for imaging quality evaluation of large space telescopes. *Sci Rep* 8, 7272 (2018).

[12] Briguglio, R. *et al.* The LATT way towards large active primaries for space telescopes. In *Space Telescopes and Instrumentation 2016*: *Optical, Infrared, and Millimeter Wave*, Vol. 9904 of Proc. of SPIE, 99041B (2016).

[13] Benisty, M., *et al*. An integrated optics beam combiner for the second generation VLTI instruments. *Astronomy & Astrophysics* 498(2): 601-613 (2009).

[14] Martinod, M.-A., *et al*. Scalable photonic-based nulling interferometry with the dispersed multi-baseline GLINT instrument. *Nature Communications* 12(1): 1-11 (2021).